PRAMANA — journal of physics

© Indian Academy of Sciences

Vol. 84, No. 6
June 2015
pp. 947–956

Electronic structure of Fe-based superconductors

KALOBARAN MAITI

Department of Condensed Matter Physics and Materials Science, Tata Institute of Fundamental Research, Homi Bhabha Road, Colaba, Mumbai 400 005, India
E-mail: kbmaiti@tifr.res.in

DOI: 10.1007/s12043-015-0992-x; ***e*Publication:** 29 May 2015

Abstract. Fe-based superconductors have drawn much attention during the last decade due to the presence of superconductivity in materials containing the magnetic element, Fe, and the coexistence of superconductivity and magnetism. Extensive study of the electronic structure of these systems suggested the dominant role of *d* states in their electronic properties, which is significantly different from the cuprate superconductors. In this article, some of our studies of the electronic structure of these fascinating systems employing high-resolution photoemission spectroscopy is reviewed. The combined effect of electron correlation and covalency reveals an interesting scenario in their electronic structure. The contribution of ligand *p* states at the Fermi level is found to be much more significant than indicated in earlier studies. Temperature evolution of the energy bands reveals the signature of transition akin to Lifshitz transition in these systems.

Keywords. Superconductivity; pnictides; photoemission; band structure.

PACS Nos 74.70.Xa; 74.25.Jb; 71.20.−b; 79.60.−i

1. Introduction

High-temperature superconductivity continued to be one of the thrust areas in condensed matter research for many decades, where most of the focus has been centred around the study of cuprate superconductors [1]. Discovery of superconductivity in Fe-based compounds [2,3] renewed great interest in the study of high-temperature superconductivity. Fe-based systems are significantly different from the cuprates. The parent compounds in cuprates are antiferromagnetic Mott insulators, where the insulating property arises due to strong electron correlation compared to the width of their conduction band. The antiferromagnetism gets suppressed with the charge carrier doping and superconductivity emerges beyond some critical doping. The normal phases of these materials exhibit a plethora of unusual behaviours such as pseudogap phase, strange metallicity etc.

On the other hand, the parent compounds of Fe-based compounds (pnictides or chalcogenides) are metals exhibiting spin density wave (SDW) phases in the ground

state. Charge carrier doping in these systems leads to superconductivity via suppression of long-range magnetic order in the parent compositions [4]. Interestingly, many of these Fe-based compounds exhibit pressure-induced superconductivity [5,6], although application of pressure usually renormalizes the hopping interaction strengths due to the compression/distortion of the real lattice without significant change in the overall carrier concentration. Most interestingly, some Fe-based compounds exhibit unusual coexistence of magnetic order and superconductivity [6,7].

Here, the experimental results of two Fe-based superconductors, $FeTe_{0.6}Se_{0.4}$ and $CaFe_2As_2$ belonging to two different classes of materials published earlier [8–10] are reviewed and common features among these materials identified. Fe(TeSe) group of compounds, popularly known as '11' systems form in anti-PbO-type crystal structure (space group $P4/nmm$) [11], and are believed to be the most correlated ones due to their large 'chalcogen height' [12] (the height of the anions from the Fe plane) [13]. The end member, FeTe, exhibits spin density wave (SDW)-type antiferromagnetic transition at 65 K [14,15] and FeSe is a superconductor below 8 K [16,17]. Homovalent substitution of Te at Se sites in FeSe leads to an increase in superconducting transition temperature T_c with a maximum T_c of 15 K for 60% Te substitutions [18], despite the fact that such substitutions often introduce disorder in the system that is expected to reduce the superconducting transition temperature T_c [19].

$CaFe_2As_2$ belongs to another class of materials known as '122' compounds and crystallizes in the $ThCr_2Si_2$-type tetragonal structure at room temperature (space group $I4/mmm$). $CaFe_2As_2$ exhibits SDW transition due to the long-range magnetic ordering of the Fe moments at $T_{SDW} = 170$ K along with a structural transition to an orthorhombic phase. High pressure [5], substitution of Fe by Co, Ni [20] and other dopants induce superconductivity in $CaFe_2As_2$. The SDW transition is found to accompany a nesting of the Fermi surface [21,22] along with a transition from two-dimensional (2D) to three-dimensional (3D) Fermi surface associated with the structural transition [23–25].

It is believed that Fe $3d$ states play dominant roles in the electronic properties of these systems in contrast to cuprates, where the doped holes possess dominant ligand $2p$ orbital character [1]. Thus, the physics of unconventional superconductors is complex due to the significant differences among different classes of materials. Here, it is shown that the ligand p electrons play a much more important role than what was anticipated. The temperature evolution of the electronic structure reveals an interesting scenario in these materials.

2. Experimental

The single crystals of $CaFe_2As_2$ were grown using Sn flux and the single crystalline sample of $FeTe_{0.6}Se_{0.4}$ [26] was grown by self flux method. The grown crystals were characterized by X-ray diffraction, Laue, Mössbauer and transmission electron microscopic (TEM) measurements establishing stoichiometric and homogeneous composition of the sample with no trace of additional Fe in the material. The X-ray diffraction pattern could be indexed to the $ThCr_2Si_2$-type body-centred tetragonal structure with the space group of $I4/mmm$. The estimated lattice parameters are $a = 3.894\ 2(8)$ Å and $c = 11.746(7)$ Å for $CaFe_2As_2$ as shown in [20]. XRD pattern of $FeTe_{0.6}Se_{0.4}$ exhibits anti-PbO-type structure

with the space group $P4/nmm$. ^{57}Fe Mössbauer spectra were recorded in transmission geometry using a conventional constant-acceleration spectrometer and isomer shifts were observed corresponding to stoichiometric $FeTe_{0.6}Se_{0.4}$ composition [18,26].

The grown crystals are flat platelet-like, which can be cleaved easily and the cleaved surface looks like a shiny mirror. Photoemission measurements were carried out using a Gammadata Scienta analyzer, R4000 WAL and monochromatic photon sources, Al $K\alpha$ ($h\nu = 1486.6$ eV), He I ($h\nu = 21.2$ eV) and He II ($h\nu = 40.8$ eV) sources. The energy resolution and angle resolution were set to 2 meV and 0.3° respectively for ultraviolet photoemission (UP) studies and the energy resolution was fixed to 350 meV for X-ray photoemission (XP) measurements. The sample was cleaved *in situ* (base pressure $<3 \times 10^{-11}$ Torr) at each temperature several times to have a clean well-ordered surface for the photoemission studies. Reproducibility of the data in both cooling and heating cycles was observed. The energy band structures of $CaFe_2As_2$ and $FeTe_{0.5}Se_{0.5}$ were calculated using full potential linearized augmented plane-wave method within the local density approximation (LDA) using Wien2k software [27]. The energy convergence was achieved using 512 k-points within the first Brillouin zone.

3. Results and discussions

As discussed above, the major difference of Fe-based superconductors with the cuprates is believed to be the character of the conduction electrons. In cuprates, the charge transfer energy (the energy required to transfer an electron from the ligand to the copper site $\Delta \approx 2$ eV) is smaller than the electron correlation strength U ($\approx$8 eV) [28]. Therefore, the Fermi level ϵ_F lies at the top of the O 2p band and the electrons close to the Fermi level possess dominant O 2p character. The electron correlation strength in Fe-pnictides is expected to be relatively smaller ($\approx$ 4 eV) [29] and the electrons close to ϵ_F were described to be dominated by Fe 3d character. This appears to be the case in the valence band spectrum of $CaFe_2As_2$ shown in figure 1a. The X-ray photoemission (XP) spectrum at 300 K exhibits four distinct features, A, B, C and D [9]. The calculated spectral functions obtained by convoluting the band structure results with the Fermi–Dirac function and resolution broadening function exhibit good representation of the experimental spectra. It is clear that the features A and B possess dominant Fe 3d contributions (dashed line), while the As 4p states (solid line) contribute primarily in the features C and D appearing at higher binding energies.

In order to obtain a better understanding of this, the electronic states close to ϵ_F are critically investigated. The LDA results in figure 1a shows that the hybridization between As 4p and Fe 3d states is strong with non-zero contribution ($\sim$3%) coming from As 4p PDOS near ϵ_F as shown by the solid circles in the figure. This is further examined experimentally in figure 1b by comparing the spectra obtained using He I and He II excitations. The atomic photoemission cross-sections for Fe 3d and As 4p at He I energy excitation are 4.833 and 3.856, and at He II are 8.761 and 0.2949, respectively [30]. These values will be somewhat different in solids. However, the trends of change in cross-sections remain almost similar even in solids and the relative intensity corresponding to As 4p states will increase significantly at He I energy compared to He II energy. The He I and He II spectra having the same resolution broadening are compared in figure 1b. If the spectral intensity

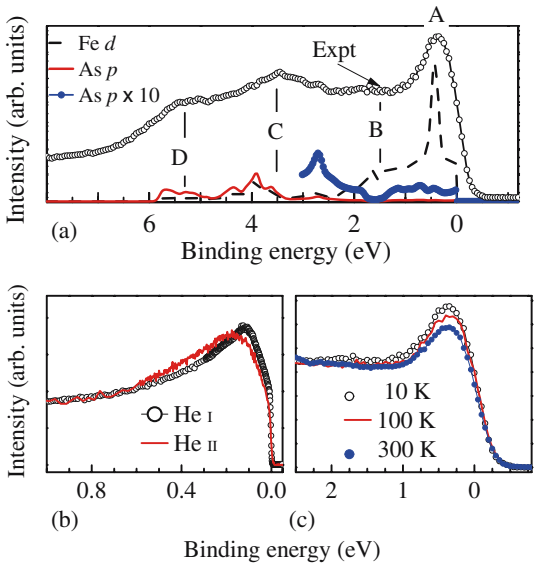

Figure 1. (**a**) XP valence band spectrum of $CaFe_2As_2$ at 300 K (symbols). Fe 3*d* and As 4*p* contributions obtained from *ab-initio* calculations are shown by dashed and solid lines. The solid circles represent the rescaled As 4*p* contributions. (**b**) Near-Fermi level feature from He I and He II excitations. (**c**) Evolution of the XP valence band spectra near ϵ_F with temperatures.

near the Fermi level is contributed by one type of electronic states, the intensity will not change with the change in photon energy. However, we observe an increase in intensity by about 15% at 100 meV binding energy in the He I spectrum relative to He II spectrum and subsequent decrease around 400 meV binding energy – the spectra are normalized by the intensity around 1 eV binding energy. This conclusively indicates that the intensities close to the Fermi level possess large As *p* character, while the intensities at higher binding energies correspond to Fe *d* contributions. This seems to be different from the conclusions of the LDA band structure results in figure 1a.

The temperature evolution of the feature A in the XP valence band spectra is shown in figure 1c after normalizing by the spectral intensities in the energy range beyond 1 eV binding energy. The intensity of the feature A exhibits gradual enhancement with the decrease in temperature, which is much beyond the temperature-induced effects due to Fermi–Dirac distribution functions. Valence band spectra of a correlated system exhibit the signature of the upper and lower Hubbard bands constituted by the correlated electronic states (often called incoherent feature). A Kondo resonance feature called coherent feature appears at the Fermi level representing the itinerant electrons. The decrease in temperature leads to an increase in the coherent feature intensity at the cost of incoherent features [31,32]. While such increase in spectral intensity can have other origin, it is strongly felt [33] that the enhancement of the feature A with the decrease in temperature shown in figure 1c can be attributed to correlation-induced effects as justified later in the text.

In figure 2a, the valence band spectra of $FeTe_{0.6}Se_{0.4}$ obtained using Al $K\alpha$ X-ray source at 10 K and 300 K after normalizing by intensities between 10 and 15 eV are

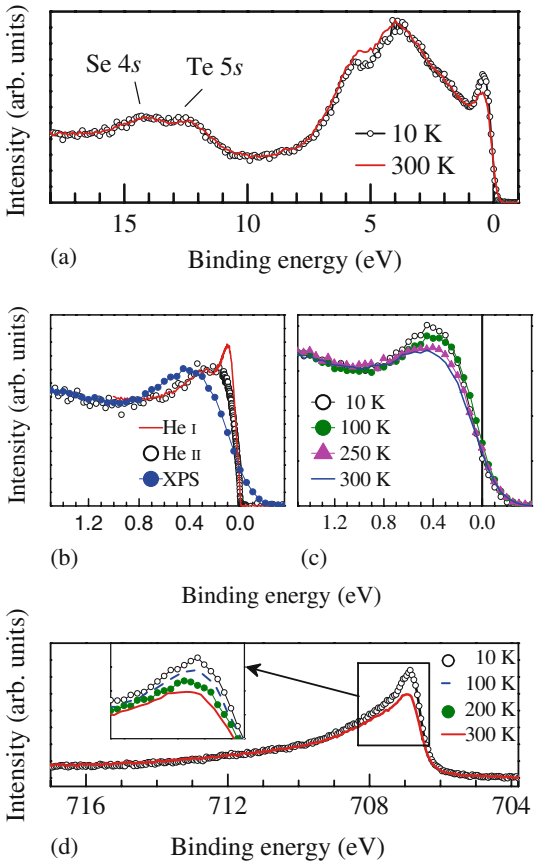

Figure 2. **(a)** XP valence band spectrum of $FeTe_{0.6}Se_{0.4}$ at 300 K (line) and 10 K (symbols). **(b)** Near-Fermi level spectra at 10 K obtained using He I, He II and Al $K\alpha$ lines at 10 K. **(c)** Temperature evolution of the near-Fermi level XP feature. **(d)** Fe 2*p* core level spectra. Inset shows expanded view of the well-screened feature.

shown [8]. The valence band exhibits multiple features – the feature close to ϵ_F possesses dominant Fe 3*d* character and Te/Se *p* related features primarily contribute in the energy range 2–7 eV as also appeared in the case of $CaFe_2As_2$. The higher binding energy (10–15 eV) features correspond to Se/Te *s* state excitations. A comparison of the near-Fermi level feature at 10 K obtained using different photon energies exhibit interesting scenario. The feature around 100 meV is most intense in the He I spectra again indicating large chalcogen *p* contributions. Decrease in temperature leads to a gradual increase in intensity of the near ϵ_F feature as shown in figure 2c consistent with the scenario in correlated electron systems.

It is to be noted here that the spectra normalized by intensities between 10 and 15 eV do not show change in intensity around 2 eV. Instead, there is a decrease in intensity around 6 eV subsequent to the increase in intensity of the feature A. Such spectral renormalization has been observed to occur due to the change in covalency [34] – the formation of lower Hubbard band leads to a spectral redistribution between the coherent and

incoherent features, and hence, the hybridization between the Fe d states and the As p states changes.

The correlation-induced effect can be verified further by inspecting the Fe 2p core level spectra shown in figure 2d. The spectra exhibit an interesting evolution with temperature. The intensity of the peak around 707 eV binding energy increases gradually with the decrease in temperature (see inset). This feature is often referred to as the well-screened feature, where the core hole created by photoemission is screened by a conduction electron in the final state [35,36]. As the decrease in temperature leads to an enhancement of the coherent feature intensity with a consequent decrease in the incoherent feature intensity [31], the core hole is expected to be more efficiently screened at lower temperatures as more mobile electrons are available at low temperatures. Therefore, the temperature evolution of the core level spectra observed here can also be attributed to the correlation-induced effect discussed for the valence band.

In order to investigate the dominance of p character near ϵ_F in the experimental spectra in contrast to the prediction of the dominance of Fe 3d states, the calculated partial density of states corresponding to the correlated and uncorrelated ground states [8] is shown. Finite electron correlation leads to a spectral weight transfer from ϵ_F to higher binding energies leading to an enhancement of the intensity around 2 eV (incoherent feature). Electron correlation affects the electronic states with different orbital characters differently depending on their degree of itineracy in the uncorrelated system [37]. This is evident in figure 3 exhibiting significant transfer of the Fe 3d partial density of states (PDOS) to higher binding energies. However, the Se 4p/Te 5p contributions increase near ϵ_F. Thus, the relative intensity of the p states near ϵ_F will be enhanced significantly with respect to the Fe d states. This explains the presence of dominant p character near ϵ_F in the experiment. After investigating the character of the electronic states near ϵ_F, the next step is the investigation of the energy band structure of a typical pnictide, $CaFe_2As_2$. All

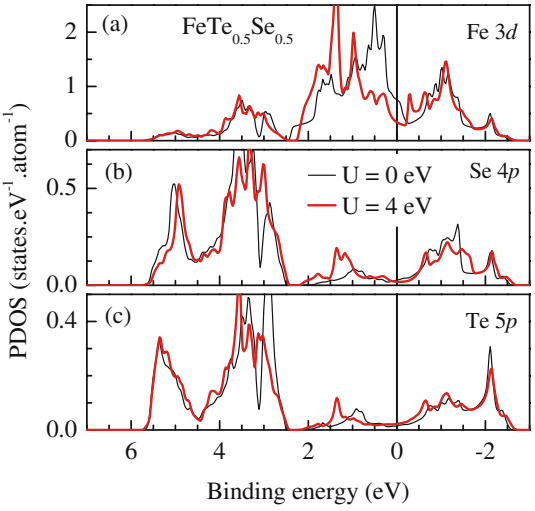

Figure 3. Calculated **(a)** Fe 3d, **(b)** Se 4p and **(c)** Te 5p partial density of states for uncorrelated (thin line for $U = 0$ eV) and correlated systems (thick line for $U = 4.0$ eV).

the samples in this class of materials exhibit essentially similar electronic structure. The calculated energy bands are shown in figure 4a exhibiting t_{2g} bands close to the Fermi level, and both bonding and antibonding e_g bands appear away from ϵ_F. Three energy bands having t_{2g} symmetry and denoted by α, β and γ in the figure cross ϵ_F near the Γ point forming three hole pockets. Here, Γ and X points are defined as $(0, 0)$ and (π, π) in the xy-plane. The k_z values corresponding to He I and He II photon energies are $k_z \sim 9.5\pi/c$ and $\sim 12.5\pi/c$, respectively.

Various angle-resolved photoemission spectroscopic measurements [23–25] show that the Fermi surface corresponding to all these three bands exhibit two-dimensional topology at room temperature, where the sample has tetragonal structure. The signatures of these three bands are observed in the momentum distribution curves (MDCs) at 300 K in the He I and He II spectra shown in figures 2b and 2c, respectively. The β- and γ-bands possessing d_{xz}, d_{yz} symmetry appear almost degenerate, while the α band having d_{xy} symmetry distinctly appears at slightly higher binding energies [9]. The energy distribution

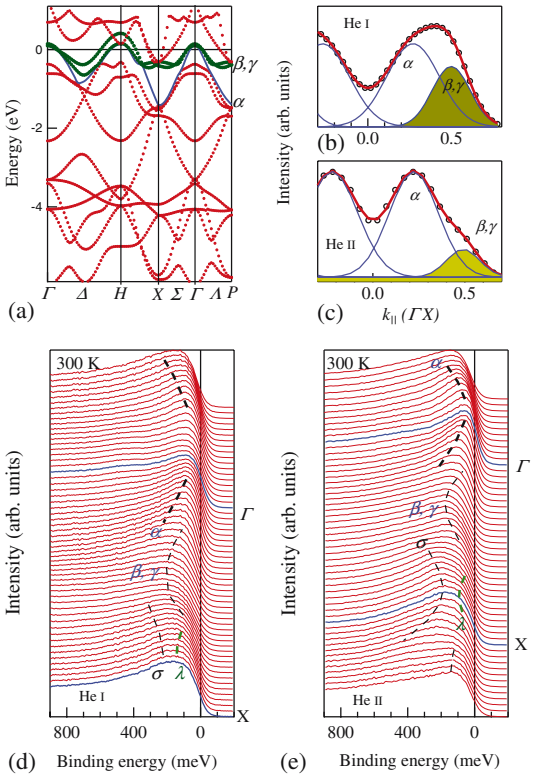

Figure 4. **(a)** Calculated energy band structure of $CaFe_2As_2$ showing three energy bands α, β and γ making three hole pockets around Γ point. Momentum distribution curves at 140 meV and 300 K in **(b)** He I and **(c)** He II spectra. The lines show typical fits exhibiting signatures of α-, β- and γ-bands. Energy distribution curves at **(d)** He I and **(e)** He II photon energies and 300 K.

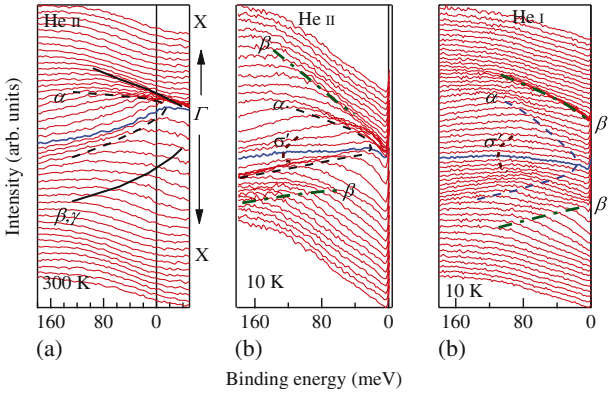

Figure 5. Energy distribution curves (EDCs) in the He II spectra at **(a)** 300 K and **(b)** 10 K. **(c)** The EDCs in the He I spectra at 10 K.

curves (EDCs) in figures 2d and 2e show that all these energy bands cross ϵ_F in the vicinity of Γ point indicating the presence of three hole pockets at room temperature. An energy band λ is also observed forming an electron pocket around X point along with the σ-band appearing at higher binding energies. While the σ-band does not play any significant role in the electronic properties, the Fermi surfaces corresponding to γ- and λ-bands are nested leading to the SDW transition in these materials [21,22].

With the decrease in temperature below the SDW transition temperature, the γ-band hole pocket and the λ-band electron pocket vanishes opening up a gap at the Fermi level [24,25]. Subsequently, the crystal structure also changes from tetragonal to orthorhombic leading to a change in the Fermi surface topology – the Fermi surface corresponding to the α-band exhibits k_z-dependence indicating its transition to three dimensionality [23]. It is observed that in the orthorhombic phase, the α-band hole pocket is centred around $k_z \sim 2(2n+1)\pi/c$ and it is absent around $4n\pi/c$ in the k-plane containing k_z-axis. Thus, α-band is expected to cross ϵ_F at He I energy, while it will appear below ϵ_F at He II energy. Figures 5a and 5b show He II EDCs at 300 K and 10 K, respectively exhibiting exactly the same scenario. Interestingly, the α-band in the He I spectra also appears below ϵ_F at 10 K as shown in figure 5c indicating the disappearance of the Fermi surface corresponding to the α-band at 10 K – larger intensity of the α-band in He II spectra compared to that in He I spectra indicate its dominant Fe 3d character.

It is to note here that many of the unconventional superconductors exhibit the signature of Lifshitz transition [38]. If the Fermi level is in proximity to a point separating hole- and electron-type Fermi surfaces, a small change in a tuning parameter such as doping, pressure would lead to a transition from an electron-type to a hole-type Fermi surface or vice versa. This is known as Lifshitz transition. Proximity to Lifshitz transition indicates significant quantum fluctuation in the system. The signature of Lifshitz transition has been observed due to subtle changes in charge carrier concentration in cuprates [38] as well as in electron-doped $Ba(Fe_{1-x}Co_x)_2As_2$ [39]. The disappearance of the hole Fermi surface corresponding to the α-band in $CaFe_2As_2$ as a function of temperature is interesting and akin to the scenario in Lifshitz transition. These results indicate the importance of Lifshitz transition in such unconventional superconductors.

4. Conclusions

In summary, here a review of our studies of the electronic structure of Fe-based superconductors $FeTe_{0.6}Se_{0.4}$ and $CaFe_2As_2$ is presented. A critical analysis of the experimental and band structure results indicates that the electronic states close to the Fermi level deriving the electronic properties of these materials possess significantly large p character. Thus, the difference between Fe-based and cuprate superconductors appears to be much less than what was thought earlier. The temperature evolution of the experimental spectra exhibit the signature of the enhancement of the coherent feature (Kondo resonance feature) at lower temperatures. The angle-resolved photoemission data from $CaFe_2As_2$ exhibit the signature of Lifshitz transition as a function of temperature.

References

[1] A Damascelli, Z Hussain and Z-X Shen, *Rev. Mod. Phys.* **75**, 473 (2003)
[2] Y Kamihara *et al*, *J. Am. Chem. Soc.* **128**, 10012 (2006)
[3] Y Kamihara, T Watanabe, M Hirano and H Hosono, *J. Am. Chem. Soc.* **130**, 3296 (2008)
[4] K Ishida, Y Nakai and H Hosono, *J. Phys. Soc. Jpn* **78**, 062001 (2009)
[5] T Park *et al*, *J. Phys.: Condens. Matter* **20**, 322204 (2008)
H Lee *et al*, *Phys. Rev. B* **80**, 024519 (2009)
S-H Baek *et al*, *Phys. Rev. Lett.* **102**, 227601 (2009)
[6] N Kurita *et al*, *Phys. Rev. B* **83**, 214513 (2011)
[7] G Adhikary *et al*, *J. Phys.: Condens. Matter* **25**, 225701 (2013)
[8] G Adhikary *et al*, *J. Appl. Phys.* **114**, 163906 (2013)
[9] G Adhikary *et al*, *J. Appl. Phys.* **115**, 123901 (2014)
[10] K Maiti *et al*, *AIP Conf. Proc.* **1512**, 15 (2013)
G Adhikary *et al*, *AIP Conf. Proc.* **1349**, 837 (2011)
G Adhikary *et al*, *AIP Conf. Proc.* **1347**, 169 (2011)
[11] M Tegel, C Löhnert and D Johrendt, *Solid-State Commun.* **150**, 383 (2010)
[12] K Kuroki, H Usui, S Onari, R Arita and H Aoki, *Phys. Rev. B* **79**, 224511 (2009)
[13] Y Mizuguchi and Y Takano, *J. Phys. Soc. Jpn* **79**, 102001 (2010)
[14] F Ma, W Ji, J Hu, Z-Y Lu and T Xiang, *Phys. Rev. Lett.* **102**, 177003 (2009)
[15] A Subedi, L Zhang, D J Singh and M H Du, *Phys. Rev. B* **78**, 134514 (2008)
[16] F-C Hsu *et al*, *Proc. Natl. Acad. Sci.* **105**, 14262 (2008)
[17] C-L Song *et al*, *Science* **332**, 1410 (2011)
[18] C S Yadav, P L Paulose and K M Subhedar, *Euro. Phys. Lett.* **90**, 27011 (2010)
[19] A Ghosal, M Randeria and N Trivedi, *Phys. Rev. B* **65**, 014501 (2001)
M Chand *et al*, *Phys. Rev. B* **85**, 014508 (2012)
[20] N Kumar *et al*, *Phys. Rev. B* **79**, 012504 (2009)
N Kumar *et al*, *Phys. Rev. B* **80**, 144524 (2009)
[21] T Kondo *et al*, *Phys. Rev. B* **81**, 060507(R) (2010)
[22] Q Wang *et al*, arXiv:1009.0271v1
[23] C Liu *et al*, *Phys. Rev. Lett.* **102**, 167004 (2009)
[24] S Thirupathaiah *et al*, *Phys. Rev. B* **84**, 014531 (2011)
[25] S de Jong *et al*, *Europhys. Letts.* **89**, 27007 (2010)
[26] C S Yadav and P L Paulose, *New J. Phys.* **11**, 103046 (2009)
[27] P Blaha, K Schwarz, G K H Madsen, D Kvasnicka and J Luitz, *WIEN2k An augmented plane wave + local orbitals program for calculating crystal properties* edited by K Schwarz (Techn. Universität Wien, Austria, 2001)

[28] K Maiti and D D Sarma, *Phys. Rev. B* **65**, 174517 (2002)
K Maiti, D D Sarma, T Mizokawa and A Fujimori, *Europhys. Lett.* **37**, 359 (1997)
K Maiti, D D Sarma, T Mizokawa and A Fujimori, *Phys. Rev. B* **57**, 1572 (1998)
[29] M Aichhorn, S Biermann, T Miyake, A Georges and M Imada, *Phys. Rev. B* **82**, 064504 (2010)
[30] J J Yeh and I Lindau, *At. Data Nucl. Data Tables* **32**, 1 (1985)
K Maiti and D D Sarma, *Phys. Rev. B* **58**, 9746 (1998)
[31] A Georges, G Kotliar, W Krauth and M J Rozenberg, *Rev. Mod. Phys.* **68**, 13 (1996)
M Imada, A Fujimori and Y Tokura, *Rev. Mod. Phys.* **70**, 1039 (1998)
[32] S Patil *et al*, *J. Phys.: Condens. Matter* **22**, 255602 (2010)
S Patil *et al*, *Phys. Rev. B* **82**, 104428 (2010)
[33] N E Sluchanko *et al*, *J. Exp. Theor. Phys.* **104**, 120 (2007)
K Maiti, V R R Medicherla, S Patil and R S Singh, *Phys. Rev. Letts.* **99**, 266401 (2007)
[34] S K Pandey and K Maiti, *Phys. Rev. B* **78**, 045120 (2008)
[35] J F van Acker *et al*, *Phys. Rev. B* **37**, 6827 (1988)
[36] M Takahashi and J-I Igarashi, *Phys. Rev. B* **85**, 085128 (2012)
K Maiti, P Mahadevan and D D Sarma, *Phys. Rev. B* **59**, 12457 (1999)
[37] R S Singh, V R R Medicherla, K Maiti and E V Sampathkumaran, *Phys. Rev. B* **77**, 201102(R) (2008)
K Maiti, *Solid-State Commun.* **149**, 1351 (2009)
[38] K-S Chen, Z Y Meng, T Pruschke, J Moreno and M Jarrell, *Phys. Rev. B* **86**, 165136 (2012)
[39] C Liu *et al*, *Nat. Phys.* **6**, 419 (2010)